The Impact of Ischemic Stress on the Quality of Isolated Pancreatic Islets

M. Goto, T. Imura, A. Inagaki, N. Ogawa, H. Yamaya, K. Fujimori, Y. Kurokawa, and S. Satomi

ABSTRACT

Background. Although the ischemic stress of donated organs has been shown to have strong negative effects on islet recovery, the impact on islet quality remains uncertain. In the present study, therefore, we examined the influence of ischemic stress on the expression of inflammatory mediators among isolated islets.

Materials and methods. Islets were isolated from adult porcine pancreata subjected to 16-hour cold ischemia time (CIT) in addition to 40-minute warm ischemia time (WIT). We evaluated the islet yield, islet loss during the first 24 hours in culture, adenosine diphosphate (ADP)/adenosine triphosphate (ATP) ratio, ATP/DNA ratio, glucose-stimulated respiratory activity, in vivo bioassay, and the expression of inflammatory mediators (tissue factor [TF], [MCP-1], macrophage migration inhibitory factor) on the isolated islets. We also analyzed ATP/DNA ratios of the exocrine tissues during isolation procedures.

Results. The islet yield, survival rate during culture, and glucose-stimulated respiratory activity were significantly lower in cases of 16-hour CIT plus 40-minute WIT compared with the control group ($P < .0001$, .0006, and .002, respectively). In contrast, ADP/ATP ratio as well as TF and MCP-1 expressions on the isolated islets were higher among the ischemic group ($P = .005$, .16, and .005, respectively). During isolation procedures, the ATP/DNA of the exocrine tissues was extremely lower in the ischemic compared to the control group ($P < .0001$). Notably, however, both ATP/DNA and ADP/ATP ratio of isolated islets were well preserved even in the ischemic group ($P = .45$ and .40).

Discussion. These data suggest that ischemic stress during the preservation period negatively affects the energy status of exocrine tissues. Destruction of the exocrine tissues, in combination with warm ischemic stress during the isolation procedures, subsequently decreases isolated islet activity, inducing the expression of inflammatory mediators.

From the Tohoku University International Advanced Research and Education Organization (M.G., T.I., A.I.), Tohoku University, Sendai, Japan; Division of Advanced Surgical Science and Technology (M.G., N.O., H.Y., S.S.), Tohoku University, Sendai, Japan; Division of Surgical Oncology (K.F.), Tohoku University, Sendai, Japan; and Tohoku University Innovation of New Biomedical Engineering Center (Y.K.), Tohoku University, Sendai, Japan.

This study has been supported by grants from Innovation Plaza Miyagi of JST (Japan Science and Technology Agency), the Japanese Grant-in-Aid for Scientific Research (B).

Address reprint requests to Masafumi Goto, MD, PhD, Tohoku University International Advanced Research and Education Organization, Tohoku University 2-1 Seiryo-machi, Aoba-ku, Sendai, Miyagi, 980-8575, Japan. E-mail: **gotokichi@aol.com**

0041-1345/10/$–see front matter
doi:10.1016/j.transproceed.2010.05.101

ALTHOUGH THE ISCHEMIC STRESS of the donated organs has a strong negative effect on islet recovery,[1–4] its impact on islet quality remains uncertain. In the present study, therefore, we examined the influence of ischemic stress on the expression of inflammatory mediators in isolated islets. Furthermore, we evaluated the impact of ischemic stress on the energy status of the pancreatic tissues. We employed scanning electrochemical microscopy, a technique in which the tip of a microelectrode monitors the local distribution of electroactive species near the sample surface, to assess islet viability and examine the potency of insulin release.

MATERIALS AND METHODS

Islets were isolated from adult porcine pancreata subjected to 16-hour cold ischemia time (CIT) in addition to 40-minute warm ischemia time (WIT). We evaluated on the isolated islets the yield, islet loss during the first 24 hours in culture, adenosine diphosphate (ADP)/adenosine triphosphate (ATP) and ATP/DNA ratios, glucose-stimulated respiratory activity, in vivo bioassay, and the expression of inflammatory mediators—tissue factor (TF), MCP-1, macrophage migration inhibitory factor. For the respiratory activity assay, we used scanning electrochemical microscopy, which automatically measured the reduced current of far and near points of the samples based upon spherical diffusion theory. The respiratory activity of 10 islets in each group was calculated by detecting the difference in the reduction current around the samples using 2- to 4-μm platinum-coated microelectrodes as described previously.[5] Glucose-stimulated respiratory activity was indicated by the stimulation index of respiratory activity, defined as the ratio of the activity in high (16.7 mmol/L) versus that in basal glucose concentrations (1.67 mmol/L). The ATP/DNA of exocrine tissues was also analyzed during isolation procedures. The ADP/ATP assays, levels of insulin/DNA, and Trypan blue exclusion tests were performed as previously described.[6,7]

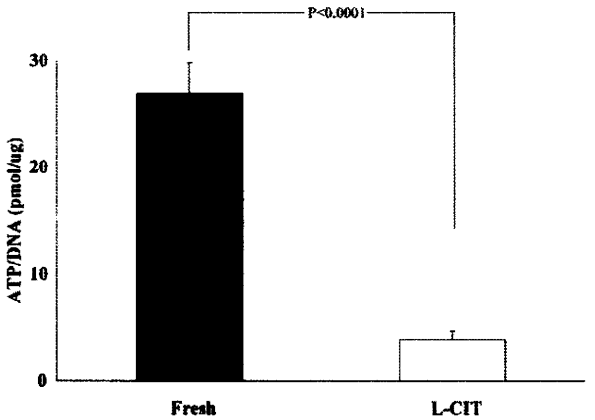

Fig 1. Energy status of the exocrine tissues during isolation procedures is shown. The y-axis indicates the adenosine triphosphate (ATP) amount per DNA in the exocrine tissues. The black bar shows fresh islets (Fresh), and the white bar shows 16-hour cold ischemia times (L-CIT). During isolation procedures, the ATP/DNA of the exocrine tissues was extremely lower in the ischemic group compared to the control group ($P <$ .0001).

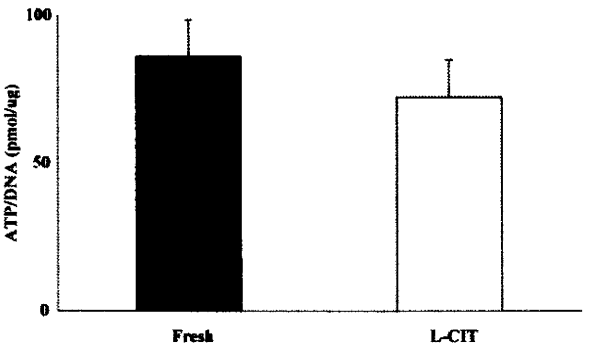

Fig 2. Energy status of the pancreatic islets during isolation procedures is shown. The y-axis indicates the adenosine triphosphate (ATP) amount per DNA in the pancreatic islets. The black bar shows fresh islets (Fresh), and the white bar shows 16-hour cold ischemia times (L-CIT). Energy status of the isolated islets was well preserved even in the ischemic group.

RESULTS

The islet yield, survival rate during culture, and glucose-stimulated respiratory activity were significantly lower among the 16-hour CIT and 40-minute WIT compared with the control group (P = .0001, .0006, and .002, respectively). In contrast, the ADP/ATP ratio as well as TF and MCP-1 expression on the isolated islets were higher in the ischemic group (P = .005, .16, and .005, respectively). During isolation procedures, the ATP/DNA in exocrine tissues was extremely less in the ischemic compared with the control group ($P <$ .0001; **Fig** 1). Notably, however, both the ATP/DNA (**Fig** 2) and ADP/ATP ratios of isolated islets were well preserved even among the ischemic group (P = .45 and .40).

DISCUSSION

The success of clinical islet isolations is less than 50% due to several reasons.[8] Ischemic stress is one of the crucial factors affecting the recovery of isolated islets. In the present study, we have shown that ischemic stress during the preservation period negatively affects the energy status of the exocrine tissues, but not of the isolated islets. Furthermore, we have also demonstrated that the expression of inflammatory mediators, such as TF and MCP-1, on isolated islets was remarkably induced in the ischemic compared with the fresh group. These data suggested that the destruction of exocrine tissues during cold preservation, in combination with warm ischemic stress during isolation procedures, could contribute to decrease islet activity possibly due to the release of proteases from exocrine tissues and subsequently induction of the expression of inflammatory mediators on the isolated islets.

ACKNOWLEDGMENTS

The authors thank Kozue Maya and Megumi Goto for their excellent technical assistance.

REFERENCES

1. Goto M, Eich TM, Felldin M, et al: Refinement of the automated method for human islet isolation and presentation of a closed system for in vitro islet culture. Transplantation 78:1367, 2004

2. Toso C, Oberholzer J, Ris F, et al: Factors affecting human islet of Langerhans isolation yields. Transplant Proc 34:826, 2002

3. Zeng Y, Torre MA, Karrison T, et al: The correlation between donor characteristics and the success of human islet isolation. Transplantation 57:954, 1994

4. Lakey JR, Warnock GL, Rajotte RV, et al: Variables in organ donors that affect the recovery of human islets of Langerhans. Transplantation 61:1047, 1996

5. Goto M, Abe H, Ito-Sasaki T, et al: A novel predictive method for assessing the quality of isolated pancreatic islets using scanning electrochemical microscopy. Transplant Proc 41:311, 2009

6. Goto M, Holgersson J, Kumagai-Braesch M, et al: The ADP/ATP ratio: a novel predictive assay for quality assessment of isolated pancreatic islets. Am J Transplant 6:2483, 2006

7. Wennberg L, Song Z, Bennet W, et al: Diabetic rats transplanted with adult porcine islets and immunosuppressed with cyclosporine A, mycophenolate mofetil, and leflunomide remain normoglycemic for up to 100 days. Transplantation 71:1024, 2001

8. Ponte GM, Pileggi A, Messinger S, et al: Toward maximizing the success rates of human islet isolation: influence of donor and isolation factors. Cell Transplant 16:595, 2007

Cell Transplantation, Vol. 19, pp. 775–782, 2010

0963-6897/10 $90.00 + .00
DOI: 10.3727/096368910X508889
E-ISSN 1555-3892
www.cognizantcommunication.com

Brain Death in Combination With Warm Ischemic Stress During Isolation Procedures Induces the Expression of Crucial Inflammatory Mediators in the Isolated Islets

Yukihiko Saito,* Masafumi Goto,*† Kozue Maya,† Norihiko Ogawa,*
Keisei Fujimori,‡ Yoshimochi Kurokawa,§ and Susumu Satomi*

*Division of Advanced Surgical Science and Technology, Tohoku University, Sendai, Japan
†Tohoku University International Advanced Research and Education Organization, Tohoku University, Sendai, Japan
‡Medical Safety Management Office, Tohoku University, Sendai, Japan
§Tohoku University Innovation of New Biomedical Engineering Center, Tohoku University, Sendai, Japan

Tissue factor (TF) and monocyte chemoattractant protein-1 (MCP-1) expressed on the islets have been identified as the main trigger of the instant blood-mediated inflammatory reaction (IBMIR) in islet transplantation. Because the key steps that directly induce TF and MCP-1 remain to be determined, we focused on the influence of brain death (BD) on TF and MCP-1 expression in the pancreatic tissues and isolated islets using a rodent model. TF and MCP-1 mRNA levels in the pancreatic tissues were similar between the BD and the control group. However, TF and MCP-1 mRNA in the fresh islets of the BD group were significantly higher than that of the control group ($p < 0.01$). BD may thus be suggested to be of great importance as an initiator of TF and MCP-1 induction in the isolated islets. Furthermore, the upregulation of crucial inflammatory mediators induced by BD could be exacerbated by warm ischemic damage during digestion procedures. In the present study, the islet yield and purity were affected by BD. However, almost no influences were observed with respect to islet viability, indicating that the expression of inflammatory mediators rather than islet viability is more susceptible to BD. According to the change in time course of TF and MCP-1 expression in the isolated islets, the selected time point for islet infusion in current clinical islet transplantation was thus shown to be at its worst level, at least with respect to the damage caused by BD and ischemic stress. In conclusion, BD in combination with warm ischemic stress during isolation procedures induces a high expression of TF and MCP-1 in the isolated islets. In order to reduce the expression of crucial inflammatory mediators in the islet grafts, the management of the pancreas from brain-dead donors with early anti-inflammatory treatments is thus warranted.

Key words: Islets; Transplantation; Brain death; Tissue factor (TF); Monocyte chemoattractant protein-1 (MCP-1)

INTRODUCTION

Islet transplantation is now becoming a viable option for the clinical treatment of type 1 diabetic patients (26,27,32). Although the Edmonton protocol introduced various suggestions for the improvement of islet transplantation, one of the most crucial messages was undoubtedly the necessity for multiple donor organs to render diabetic patient insulin independent. In other words, the Edmonton protocol could be regarded as a refined dose-finding study for the amount of islets needed to cure diabetes. Therefore, in order for islet transplantation to become a widespread standard therapy, diabetes reversal must be achieved with a single donor to reduce the risks and costs, and to increase the availability of transplantation.

However, it is well known that a large part of the transplanted islets tend to be destroyed immediately after transplantation. One of the possible explanations for the poor outcome is the instant blood-mediated inflammatory reaction (IBMIR), which is an innate immune response during islet engraftment (4). Our group, as well as others, have showed that tissue factor (TF) and monocyte chemoattractant protein-1 (MCP-1) expressed on the grafted islets elicit an injurious IBMIR when the islets come into direct contact with the blood

Received June 1, 2009; final acceptance April 21, 2010. Online prepub date: June 23, 2010.
Address correspondence to Masafumi Goto, M.D., Ph.D., Tohoku University International Advanced Research and Education Organization, Tohoku University, 2-1 Seiryo-machi, Aoba-ku, Sendai, Miyagi, 980-8575, Japan. Tel: +81 22 717 7895; Fax: +81 22 717 7899; E-mail: gotokichi@aol.com

stream (5,11,17,21,23). Therefore, in order to improve the outcome of clinical islet transplantation, the expression of these crucial inflammatory mediators in the isolated islets should be reduced prior to transplantation.

It is well known that the result of organ transplantation is highly influenced by brain death (BD) (31). In the field of islet transplantation, it was reported by Contreras et al. that BD upregulated the proinflammatory cytokines, such as tumor necrosis factor-α (TNF-α, interleukin-1β (IL-1β), and IL-6 in the serum and pancreatic tissues (6). Toyama et al. also demonstrated that TNF-α, IL-1β, IL-6, and MCP-1 were activated in the isolated islets from rodent BD donors (33). However, the influence of BD on the TF expression in the isolated islets still remains uncertain.

Furthermore, in islet transplantation, unlike other organ transplantation, the islet grafts are placed under hypoxic condition at 37°C during the whole digestion procedure. This period is theoretically considered as one kind of severe warm ischemia (2,12,28).

In the present study, we therefore analyzed the influence of BD on the expression of TF and MCP-1 in both the pancreatic tissues and the isolated islets, in order to understand the key steps that induce crucial inflammatory mediators in the islet grafts.

MATERIALS AND METHODS

Rodent Brain Death Model

All the animals in this study were handled in accordance with the *Guide for the Care and Use of Laboratory Animals* published by the National Institutes of Health (3) and the guidelines for animal experiment and related activities at Tohoku University. BD was induced in male Lewis rats weighing 250–300 g by inflation of a No. 3 Fogarty catheter (Edwards Lifesciences Corporation, Irvine, CA, USA) placed intracranially, as previously described (6,24). Briefly, anesthesia was induced with diethleter and maintained by the IP administration of pentobarbital sodium, Nembutal (Abbott Laboratories, Abbott Park, IL, USA) at a dose of 30 mg/kg. A No. 3 Fogarty catheter was inserted through a 1-mm hole drilled through the skull at 3 mm lateral to the sagittal suture. For the gradual rise in the intracranial pressure, the balloon was inflated with 40 μl/min of distilled water until respiration ceased. The absence of refluxes, apnea, and the maximally dilated and fixed pupils confirmed the condition. The average balloon volume for making BD was 210 μl. The rats were tracheotomized for intubation and mechanically respirated (respiratory rate: 60/min, tidal volume: 10 ml/kg) with SAR-830 Ventilator (CWE, Inc., Ardmore, PA, USA) for 6 h until the removal of the pancreas. The arterial blood pressure was monitored continuously via 24G SURFLO I.V. Catheters (TERUMO, Tokyo, Japan) placed into the right femoral artery and attached to a Dynascope (Fukuda Denshi, Tokyo, Japan). In order to avoid the ischemic effects, the mean arterial pressure (MAP) was maintained over 80 mmHg. When the MAP fell under 80 mmHg during the maintenance of BD, the balloon volume was reduced by 10 μl/min until the animal became normotensive. During the 6-h period, 6 ml/kg/h of normal saline solution was administered IV. The control rats were anesthetized and tracheotomized using the same method. Thereafter, a Fogarty catheter was inserted without ballooning. The control rats were not mechanically respirated because sustained anesthesia was needed for the 6-h ventilation.

Islet Isolation and Culture

Before the removal of the pancreas, the cannulated bile duct was injected with 10 ml of cold Hanks' balanced salt solutions (HBSS) containing 1 g/L collagenase (Sigma type V; Sigma Chemicals, St. Louis, MO, USA). After the addition of 10 ml HBSS, the pancreas was digested at 37°C for 14 min. Thereafter, density-gradient centrifugation was performed using Histopaque-1119 (Sigma Diagnostics, St. Louis, MO, USA) and Lymphoprep™ (Nycomed Pharma AS, Oslo, Norway) to isolate the pancreatic islets. The islet count was performed as islet equivalents (IEQs) under a scaled microscope using diphenylthiocarbazone (Wako, Osaka, Japan) staining (BD, $n = 8$; control, $n = 7$). One IEQ was the islet mass equivalent to a spherical islet of 150 μm in diameter. The islets were cultured in RPMI-1640 containing 5.5 mmol/L glucose and 10% fetal bovine serum at 37°C in 5% CO_2 and humidified air before examination.

Islet Viability and Function

The adenosine triphosphate (ATP)/deoxyribonucleic acid (DNA) ratio was measured to evaluate both the energy status of the isolated islets after 3 h (BD, $n = 4$; control, $n = 4$) and the overnight culture (BD, $n = 6$; control, $n = 5$). A total of 80 IEQs of the islets were used in both groups. The ApoGlow™ kit (Lonza Rockland Inc., Rockland, ME, USA) was used for the ATP measurements as described previously (10). Using the same sample, the DNA content was measured using the DNA Quantify kit (Primary cell, Sapporo, Japan) as described previously (34). We have evaluated the respiratory activity of the isolated islets after 3 h (BD, $n = 4$; control, $n = 4$) and of the overnight culture (BD, $n = 6$; control, $n = 5$) using scanning electrochemical microscopy. The stimulation index of the respiratory activity, defined as the ratio of the respiratory activity in the high glucose (16.7 mmol/L) to that in the basal glucose (1.67 mmol/L), is a novel marker that could be applied as a

rapid and potent predictor for the outcome of clinical islet transplantation (8).

Determination of TF and MCP-1 mRNA in the Pancreatic Tissues

The pieces of the pancreatic tissues from the BD and the control groups were snap-frozen in liquid nitrogen and stored at −80°C until further use ($n = 6$ and $n = 4$, respectively). The total RNA was extracted using the RNeasy Mini Kit (Qiagen, Tokyo, Japan) according to the manufacturer's protocol. The RNA concentration was estimated from the absorbance at 260 nm. The first-strand complementary DNA (cDNA) was synthesized from 2500 ng of total RNA using the Transcriptor First Strand cDNA Synthesis Kit (Roche Diagnostics, Indianapolis, IN, USA). The cDNAs were amplified by the polymerase chain reaction (PCR) using a rat TF primer and a probe, rat MCP-1 primer probe set (Nihon Gene Research Laboratories Inc., Sendai, Japan), and rat glyceraldehydes-3-phosphate dehydrogenase (GAPDH) primer probe set (Nihon Gene Research Laboratories Inc.) with a Lightcycler (Roche Diagnostics). The primer sequences of the rat TF from the 5′ to 3′ direction were as follows: forward, AGC TAC TGC TTC TTC GTA CA; reverse, AAA GAC AGT GAC CAG GAA CA. The hybridization (FRET) probe sequences from 5′ to 3′ direction were as follows: TCC CAG GAC ACT CTT CCA TTG CTC AGT G-Fluorescein; LC Red 640-ACT TGG TGA TGC TTT CTG GGC TCT TGT G-phosphorylation. In order to perform the PCR for TF and GAPDH, an initial denaturation step of 10 min at 95°C was followed by 40 cycles of 10 s at 95°C, an annealing of 15 s at 60°C, and extension of 7 s at 72°C. For MCP-1, an initial denaturation step of 10 min at 95°C was followed by 40 cycles of 10 s at 95°C, an annealing of 15 s at 62°C, and extension of 6 s at 72°C.

Determination of TF and MCP-1 mRNA in the Fresh Isolated Islets

The total RNA extracted from 300 IEQs of islets with a 3-h culture was prepared using the RNeasy Micro Kit (Qiagen) according to the manufacturer's protocol (BD, $n = 3$; control, $n = 3$). The RNA concentration was estimated from the absorbance at 260 nm. The first-strand cDNA was synthesized from 100 ng of total RNA using the Transcriptor First Strand cDNA Synthesis Kit (Roche Diagnostics). The cDNAs were amplified by PCR using the rat TF primer and a probe, rat MCP-1

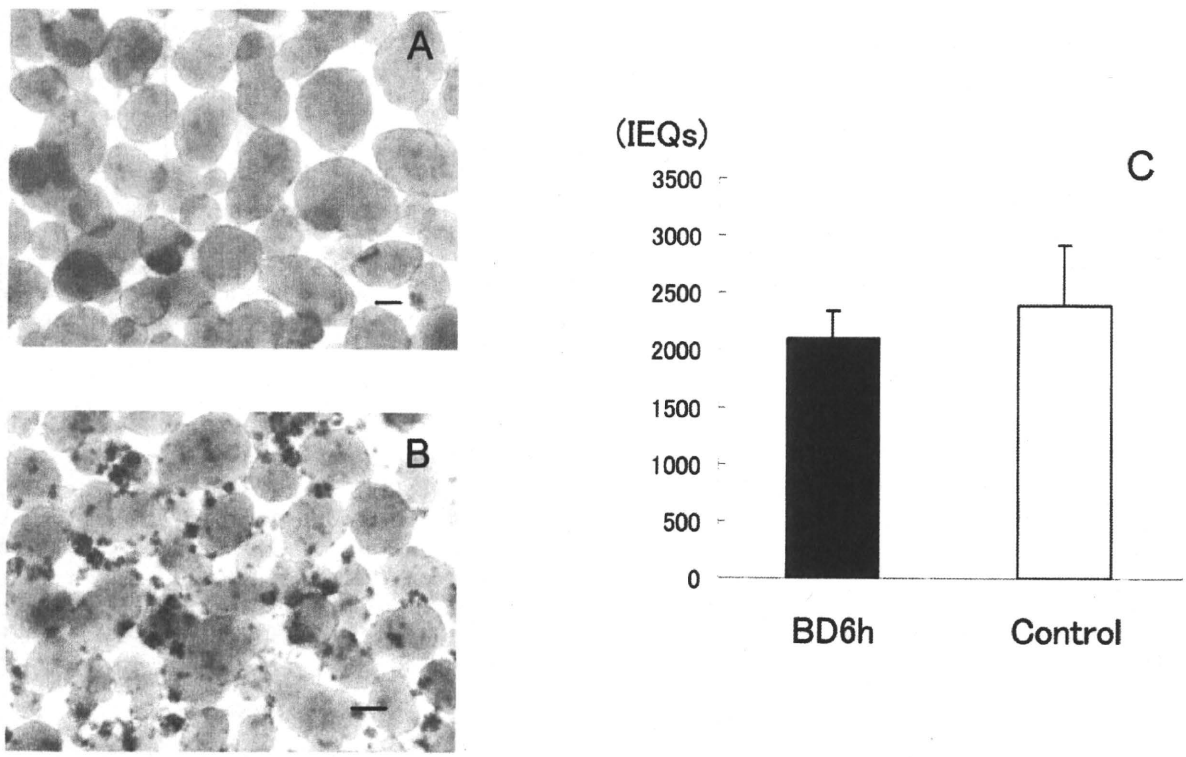

Figure 1. Islet recovery and purity after isolation. The appearance of the isolated islets without brain death (A) and with brain death (B). Scale bar: 100 μm. (C) The isolated islet yield from brain-dead donors (black bar) and control donors (white bar).

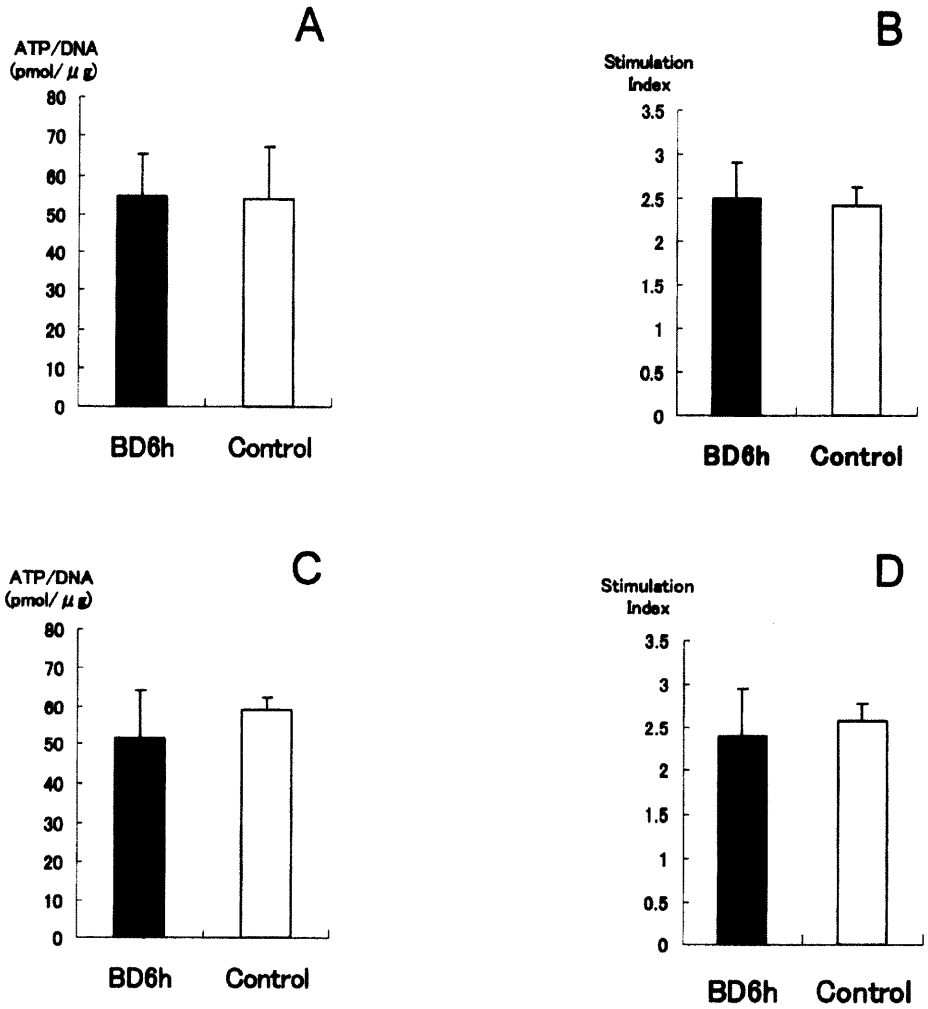

Figure 2. Islet viability and function after isolation. The ATP/DNA ratio in the fresh isolated islets (A) and in the overnight-cultured islets (C). The stimulation index of the respiratory activity in the fresh isolated islets using scanning electrochemical microscopy (B) and in the overnight-cultured islets (D). The black bar represents the brain-dead donors and the white bar represents the control donors.

primer probe set, and rat GAPDH primer probe set with a Lightcycler. The primer and probe sequences and the PCR conditions were the same as above.

Time Course Change of TF and MCP-1 mRNA Expression in the Isolated Islets

The isolated islets from one donor were divided equally into seven groups (BD, $n = 3$; control, $n = 4$). Each group was cultured for 3, 6, 12, 18, 24, 48, and 72 h, respectively. Just before examination, the cultured islets were handpicked for preparation. The TF and MCP-1 mRNA in each group were analyzed using the same procedure as above.

Statistical Analyses

All the data are expressed as the mean ± SD. The comparisons between two groups were performed by using the Student *t*-test. One-factor ANOVA with Bonferroni-Dunn post hoc test was used to determine the time course effect of the TF and MCP-1 expression in the isolated islets. Statistical significance was established at $p < 0.05$.

RESULTS

Islet Recovery and Purity After Isolation

The islet yield was considerably lower (BD, 2110 ± 231 IEQs; control, 2390 ± 528 IEQs; $p = 0.19$), and the

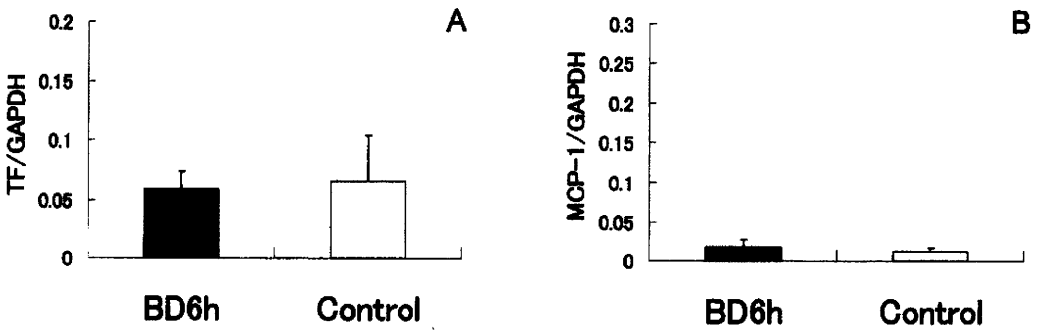

Figure 3. The mRNA expression of TF and MCP-1 in the pancreatic tissues. The mRNA expression of TF (A) and MCP-1 (B) in the pancreatic tissues from the donors with/without brain death was analyzed using a real-time PCR assay. The black bar represents the brain-dead donors and the white bar represents the control donors.

purity was significantly lower in the BD group in comparison to the control group (BD 87.7 ± 7.5%; control 97.0 ± 2.6%; $p = 0.002$) (Fig. 1).

Islet Viability and Function After Isolation

Unexpectedly, the ATP/DNA ratio and the respiratory activity were comparable between the groups, irrespective of the time point (ATP/DNA 3-h BD 54.7 ± 10.7; control 54.0 ± 13.3, $p = 0.94$; ATP/DNA overnight BD 51.6 ± 12.8; control 59.1 ± 3.47, $p = 0.20$; respiratory activity 3-h BD 2.50 ± 0.41; control 2.42 ± 0.21, $p = 0.74$; respiratory activity overnight BD 2.39 ± 0.55; control 2.58 ± 0.19, $p = 0.45$) (Fig. 2).

mRNA Expression of TF and MCP-1 in the Pancreatic Tissues

The TF and MCP-1 mRNA levels in the pancreatic tissues prior to the isolation procedures were similar between the BD and control groups (TF/GAPDH BD 0.059 ± 0.015; control 0.066 ± 0.038, $p = 0.67$, MCP-1/GAPDH BD 0.018 ± 0.0098; control 0.012 ± 0.0040, $p = 0.40$) (Fig. 3).

mRNA Expression of TF and MCP-1 in the Fresh Isolated Islets

The TF mRNA levels in the fresh isolated islets of the BD group was significantly higher in comparison to the control group (TF/GAPDH BD 0.148 ± 0.010; control 0.061 ± 0.0096, $p = 0.0004$). The MCP-1 mRNA levels in the fresh isolated islets of the BD group was also significantly higher in comparison to the control group (MCP-1/GAPDH BD 0.240 ± 0.035; control 0.140 ± 0.0070, $p = 0.008$) (Fig. 4).

Time Course Change of TF and MCP-1 mRNA Expression in the Isolated Islets

In the fresh islets, a sharp difference was observed between the BD and the control groups with respect to

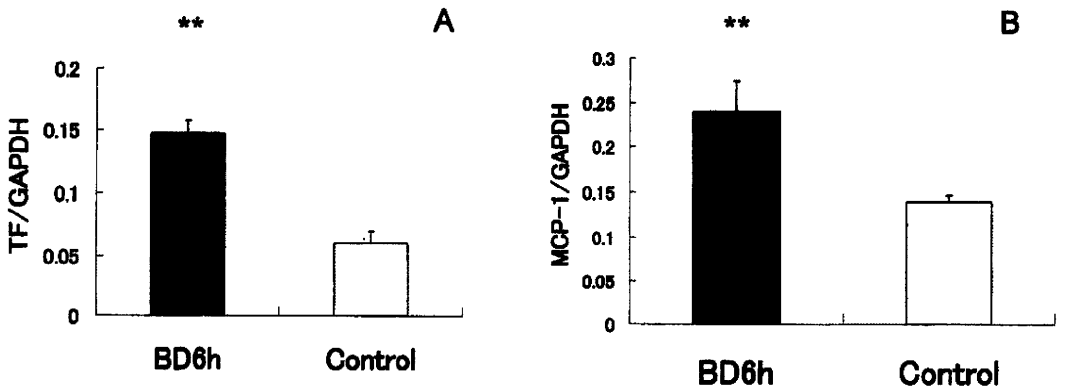

Figure 4. The mRNA expression of TF and MCP-1 in the fresh isolated islets. The mRNA expression of TF (A) and MCP-1 (B) in the fresh isolated islets from the donors with/without brain death was analyzed using a real-time PCR assay (**$p < 0.01$ vs. control). The black bar represents the brain-dead donors and the white bar represents the control donors.

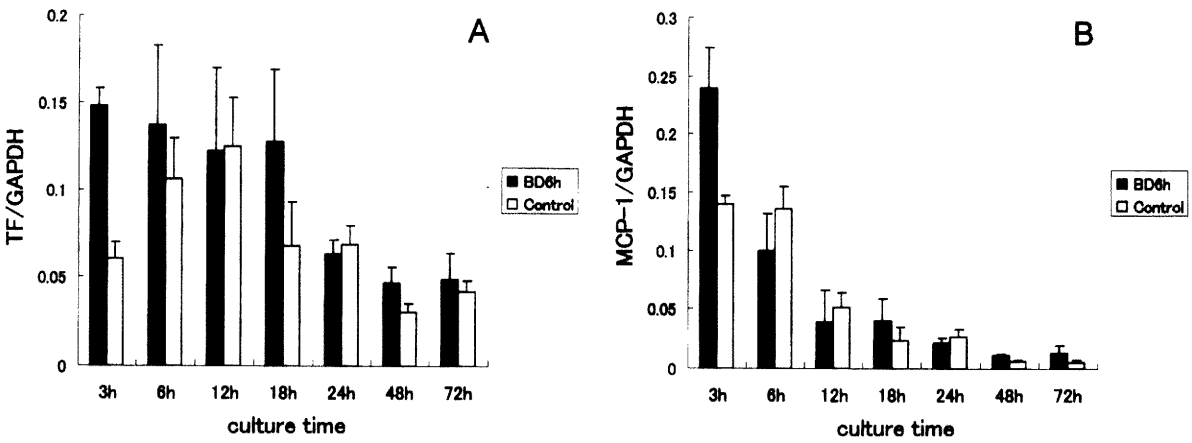

Figure 5. The change in time course of the TF and MCP-1 mRNA expression in the isolated islets. The change in time course of the TF (A) and MCP-1 (B) mRNA expression in the isolated islets from the donors with/without brain death. The black bar represents the brain-dead donors and the white bar represents the control donors. A significant difference was observed in the TF expression in the islets from the brain-dead donors between the 3- and 48-h cultures ($p < 0.05$).

the TF and MCP-1 mRNA expression. In both groups, the TF and MCP-1 mRNA levels decreased time dependently during the culture period. Between the fresh and the 48-h culture, a significant difference was seen in the TF expression in the islets from the BD donors ($p < 0.05$) (Fig. 5).

DISCUSSION

This study demonstrated that BD influences the TF and MCP-1 expressions in the isolated islets but not in the pancreatic tissues prior to the digestion procedure. It is possible that the difference may be attributed to the warm ischemic stress during the digestion procedures. However, TF and MCP-1 were not upregulated in the isolated islets from the donors without BD, thus suggesting that the warm ischemic damage per se during the digestion procedure was not sufficient to induce crucial inflammatory mediators in the islet grafts. We therefore believe that upregulation of the crucial inflammatory mediators induced by BD could be further exacerbated by warm ischemic damage during the digestion procedure.

In the present study, the islet yield and purity were certainly affected by BD. However, the difference was extremely low in comparison to the previous report (6). Moreover, almost no influences were observed in terms of the islet viability. One of the possible explanations for this discrepancy is the difference of the isolation procedure. In our methods, the pancreatic tissues were kept on ice during the whole procedure, with the exception of the digestion phase. Furthermore, at the density-gradient centrifugation phase, we applied Histopaque-1119 and Lymphoprep™. However, a dextran gradient separation was performed in the previous report (6). Therefore, the important message from our present study is that the expression of the inflammatory mediators, rather than the islet viability, is more susceptible to BD. In other words, it seems more likely that the current standard methods for the islet quality assessment are not suitable tools for detecting graft damage in the early phase of islet transplantation.

Although the islet culture modulated the inflammatory status of the human pancreatic islets (19,20), the effect remains controversial. We therefore investigated the change in time course of the TF and MCP-1 expressions in the isolated islets with/without BD. As shown in Figure 5, the influence of BD and ischemic stress during the isolation procedure was most pronounced after a 3-h culture. Clinical islet transplantation is currently being performed in most institutions, using fresh islets according to the Edmonton protocol (26,27). Notably, in most clinical cases, the islet grafts with a 3-h culture are used in fresh islet transplantation because several quality tests and preparation for graft injections are needed. Therefore, the present study clearly showed that the worst time point was selected for islet infusion in current clinical islet transplantation, at least with respect to the damage due to BD and ischemic stress during the isolation procedure.

One way to avoid the adverse effect of BD and ischemic stress is by performing short-term culture of the islet grafts. This may be one of the possible explanations for the outstanding result of the clinical islet transplantation reported by Froud et al. (7) and by Hering et al. (14). In support of our previous findings (30), the present study also implied that the TF expression in the islets without BD was substantially upregulated during overnight culturing. The reason for this is uncertain but the hypoxic

condition during culturing may at least be partially responsible for the TF induction (1,13,25). Taking into account this finding, it is most likely that the 48-h culture introduced in the previous reports (7,14) was reasonable. However, it was also reported that the number and function of the isolated islets may decreased after a short-term culture (9,15,16,18,22). This is consistent with our previous findings that isolated islets without culture are more beneficial to the transplant outcome under a current style of culture (29). Moreover, it may be difficult to maintain an adequate number of islets from the marginal donors after substantial periods of culturing, especially in Japan, where only non-heart-beating donors are available for islet transplantation. Therefore, further improvements are required to maintain the number and function of the cultured islets.Another way to avoid the adverse effect of BD and ischemic stress is to establish effective anti-inflammatory treatments through whole steps from the intensive care unit to the digestion procedure.

In conclusion, BD in combination with warm ischemic stress during the isolation procedures induces high expression of TF and MCP-1 in the isolated islets. In order to reduce the expression of the crucial inflammatory mediators in the islet grafts, the management of the pancreas from brain-dead donors with early anti-inflammatory treatments is warranted.

ACKNOWLEDGMENTS: We thank Takehiro Imura and Megumi Goto for their excellent technical assistance. This study has been supported by grants from Innovation Plaza Miyagi of JST (Japan Science and Technology Agency), the Japanese Grant-in-Aid for Scientific Research (B), the Ministry of Health, Labour, and Welfare, Japan, the Nakajima Foundation, and Takeda Foundation.

REFERENCES

1. Amirkhosravi, A.; Meyer, T.; Warnes, G.; Amaya, M.; Malik, Z.; Biggerstaff, J. P.; Siddiqui, F. A.; Sherman, P.; Francis, J. L. Pentoxifylline inhibits hypoxia-induced upregulation of tumor cell tissue factor and vascular endothelial growth factor. Thromb. Haemost. 80:598–602; 1998.
2. Avila, J. G.; Wang, Y.; Barbaro, B.; Gangemi, A.; Qi, M.; Kuechle, J.; Doubleday, N.; Doubleday, M.; Churchill, T.; Salehi, P.; Shapiro, J.; Philipson, L. H.; Benedetti, E.; Lakey, J. R.; Oberholzer, J. Improved outcomes in islet isolation and transplantation by the use of a novel hemoglobin-based O2 carrier. Am. J. Transplant. 6:2861–2870; 2006.
3. Bayne, K. Revised guide for the care and use of laboratory animals. Physiologist 39(4):199, 208–211; 1996.
4. Bennet, W.; Sundberg, B.; Groth, C. G.; Brendel, M. D.; Brandhorst, D.; Brandhorst, H.; Bretzel, R. G.; Elgue, G.; Larsson, R.; Nilsson, B.; Korsgren, O. Incompatibility between human blood and isolated islets of Langerhans: A finding with implications for clinical intraportal islet transplantation? Diabetes 48:1907–1914; 1999.
5. Berman, D. M.; Cabrera, O.; Kenyon, N. M.; Miller, J.; Tam, S. H.; Khandekar, V. S.; Picha, K. M.; Soderman, A. R.; Jordan, R. E.; Bugelski, P. J.; Horninger, D.; Lark, M.; Davis, J. E.; Alejandro, R.; Berggren, P. O.; Zimmerman, M.; O'Neil, J. J.; Ricordi, C.; Kenyon, N. S. Interference with tissue factor prolongs intrahepatic islet allograft survival in a nonhuman primate marginal mass model. Transplantation 84:308–315; 2007.
6. Contreras, J. L.; Eckstein, C.; Smyth, C. A.; Sellers, M. T.; Vilatoba, M.; Bilbao, G.; Rahemtulla, F. G.; Young, C. J.; Thompson, J. A.; Chaudry, I. H.; Eckhoff, D. E. Brain death significantly reduces isolated pancreatic islet yields and functionality in vitro and in vivo after transplantation in rats. Diabetes 52:2935–2942; 2003.
7. Froud, T.; Ricordi, C.; Baidal, D. A.; Hafiz, M. M.; Ponte, G.; Cure, P.; Pileggi, A.; Poggioli, R.; Ichii, H.; Khan, A.; Ferreira, J. V.; Pugliese, A.; Esquenazi, V. V.; Kenyon, N. S.; Alejandro, R. Islet transplantation in type 1 diabetes mellitus using cultured islets and steroid-free immunosuppression: Miami experience. Am. J. Transplant. 5:2037–2046; 2005.
8. Goto, M.; Abe, H.; Ito-Sasaki, T.; Inagaki, A.; Ogawa, N.; Fujimori, K.; Kurokawa, Y.; Matsue, T.; Satomi, S. A novel predictive method for assessing the quality of isolated pancreatic islets using scanning electrochemical microscopy. Transplant. Proc. 41:311–313; 2009.
9. Goto, M.; Eich, T. M.; Felldin, M.; Foss, A.; Kallen, R.; Salmela, K.; Tibell, A.; Tufveson, G.; Fujimori, K.; Engkvist, M.; Korsgren, O. Refinement of the automated method for human islet isolation and presentation of a closed system for in vitro islet culture. Transplantation 78: 1367–1375; 2004.
10. Goto, M.; Holgersson, J.; Kumagai-Braesch, M.; Korsgren, O. The ADP/ATP ratio: A novel predictive assay for quality assessment of isolated pancreatic islets. Am. J. Transplant. 6:2483–2487; 2006.
11. Goto, M.; Johansson, U.; Eich, T. M.; Lundgrem, T.; Engkvist, M.; Felldin, M.; Foss, A.; Kallen, R.; Salmela, K.; Tibell, A.; Tufveson, G.; Nilsson, B.; Korsgren, O. Key factors for human islet isolation and clinical transplantation. Transplant. Proc. 37:1315–1316; 2005.
12. Goto, T.; Tanioka, Y.; Sakai, T.; Terai, S.; Kamoda, Y.; Li, S.; Tanaka, T.; Tsujimura, T.; Matsumoto, I.; Fujino, Y.; Suzuki, Y.; Kuroda, Y. Application of the two-layer method on pancreas digestion results in improved islet yield and maintained viability of isolated islets. Transplantation 83:754–758; 2007.
13. Herbert, J. M.; Corseaux, D.; Lale, A.; Bernat, A. Hypoxia primes endotoxin-induced tissue factor expression in human monocytes and endothelial cells by a PAF-dependent mechanism. J. Cell. Physiol. 169:290–299; 1996.
14. Hering, B. J.; Kandaswamy, R.; Ansite, J. D.; Eckman, P. M.; Nakano, M.; Sawada, T.; Matsumoto, I.; Ihm, S. H.; Zhang, H. J.; Parkey, J.; Hunter, D. W.; Sutherland, D. E. Single-donor, marginal-dose islet transplantation in patients with type 1 diabetes. JAMA 293:830–835; 2005.
15. Holmes, M. A.; Clayton, H. A.; Chadwick, D. R.; Bell, P. R.; London, N. J.; James, R. F. Functional studies of rat, porcine, and human pancreatic islets cultured in ten commercially available media. Transplantation 60:854–860; 1995.
16. Ihm, S. H.; Matsumoto, I.; Zhang, H. J.; Ansite, J. D.; Hering, B. J. Effect of short-term culture on functional and stress-related parameters in isolated human islets. Transpl. Int. 22:207–216; 2009.
17. Johansson, H.; Lukinius, A.; Moberg, L.; Lundgren, T.; Berne, C.; Foss, A.; Felldin, M.; Kallen, R.; Salmela, K.; Tibell, A.; Tufveson, G.; Ekdahl, K. N.; Elgue, G.; Korsgren, O.; Nilsson, B. Tissue factor produced by the endo-

crine cells of the islets of Langerhans is associated with a negative outcome of clinical islet transplantation. Diabetes 54:1755–1762; 2005.
18. King, A.; Lock, J.; Xu, G.; Bonner-Weir, S.; Weir, G. C. Islet transplantation outcomes in mice are better with fresh islets and exendin-4 treatment. Diabetologia 48:2074–2079; 2005.
19. Lund, T.; Fosby, B.; Korsgren, O.; Scholz, H.; Foss, A. Glucocorticoids reduce pro-inflammatory cytokines and tissue factor in vitro and improve function of transplanted human islets in vivo. Transpl. Int. 21:669–678; 2008.
20. Marzorati, S.; Antonioli, B.; Nano, R.; Maffi, P.; Piemonti, L.; Giliola, C.; Secchi, A.; Lakey, J. R.; Bertuzzi, F. Culture medium modulates proinflammatory conditions of human pancreatic islets before transplantation. Am. J. Transplant. 6:2791–2795; 2006.
21. Moberg, L.; Johansson, H.; Lukinius, A.; Berne, C.; Foss, A.; Kallen, R.; Ostraat, O.; Salmela, K.; Tibell, A.; Tufveson, G.; Elgue, G.; Nilsson Ekdahl, K.; Korsgren, O.; Nilsson, B. Production of tissue factor by pancreatic islet cells as a trigger of detrimental thrombotic reactions in clinical islet transplantation. Lancet 360:2039–2045; 2002.
22. Olsson, R.; Carlsson, P. O. Better vascular engraftment and function in pancreatic islets transplanted without prior culture. Diabetologia 48:469–476; 2005.
23. Piemonti, L.; Leone, B. E.; Nano, R.; Saccani, A.; Monti, P.; Maffi, P.; Bianchi, G.; Sica, A.; Peri, G.; Melzi, R.; Aldrighetti, L.; Secchi, A.; Di Carlo, V.; Allavena, P.; Bertuzzi, F. Human pancreatic islets produce and secrete MCP-1/CCL2: Relevance in human islet transplantation. Diabetes 51:55–65; 2002.
24. Pratschke, J.; Wilhelm, M. J.; Kusaka, M.; Laskowski, I.; Tilney, N. L. A model of gradual onset brain death for transplant-associated studies in rats. Transplantation 69: 427–430; 2000.
25. Rong, Y.; Post, D. E.; Pieper, R. O.; Durden, D. L.; Van Meir, E. G.; Brat, D. J. PTEN and hypoxia regulate tissue factor expression and plasma coagulation by glioblastoma. Cancer Res. 65:1406–1413; 2005.
26. Ryan, E. A.; Lakey, J. R.; Rajotte, R. V.; Korbutt, G. S.; Kin, T.; Imes, S.; Rabinovitch, A.; Elliott, J. F.; Bigam, D.; Kneteman, N. M.; Warnock, G. L.; Larsen, I.; Shapiro, A. M. Clinical outcomes and insulin secretion after islet transplantation with the Edmonton protocol. Diabetes 50: 710–719; 2001.
27. Shapiro, A. M.; Lakey, J. R.; Ryan, E. A.; Korbutt, G. S.; Toth, E.; Warnock, G. L.; Kneteman, N. M.; Rajotte, R. V. Islet transplantation in seven patients with type 1 diabetes mellitus using a glucocorticoid-free immunosuppressive regimen. N. Engl. J. Med. 343:230–238; 2000.
28. Swift, S.; Kin, T.; Mirbolooki, M.; Wilson, R.; Lakey, J. R. Comparison of cooling systems during islet purification. Cell Transplant. 15:175–180; 2006.
29. Takahashi, H.; Goto, M.; Ogawa, N.; Saito, Y.; Fujimori, K.; Kurokawa, Y.; Doi, H.; Satomi, S. Superiority of fresh islets compared with cultured islets. Transplant. Proc. 41: 350–351; 2009.
30. Takahashi, H.; Goto, M.; Ogawa, N.; Saito, Y.; Fujimori, K.; Kurokawa, Y.; Doi, H.; Satomi, S. Influence of a current style of culture on the quality of isolated pancreatic islets. Transplant. Proc. 40:358–359; 2008.
31. Terasaki, P. I.; Cecka, J. M.; Gjertson, D. W.; Takemoto, S. High survival rates of kidney transplants from spousal and living unrelated donors. N. Engl. J. Med. 333:333–336; 1995.
32. The CITR Group. 2007 Update on allogeneic islet transplantation from the Collaborative Islet Transplant Registry (CITR). Cell Transplant. 18(7):753–767; 2009.
33. Toyama, H.; Takada, M.; Suzuki, Y.; Kuroda, Y. Activation of macrophage-associated molecules after brain death in islets. Cell Transplant. 12:27–32; 2003.
34. Wennberg, L.; Song, Z.; Bennet, W.; Zhang, J.; Nava, S.; Sundberg, B.; Bari, S.; Groth, C. G.; Korsgren, O. Diabetic rats transplanted with adult porcine islets and immunosuppressed with cyclosporine A, mycophenolate mofetil, and leflunomide remain normoglycemic for up to 100 days. Transplantation 71:1024–1033; 2001.

doi:10.1093/brain/awr038 Brain 2011: 134; 1089–1100 | 1089

BRAIN
A JOURNAL OF NEUROLOGY

^{18}F-THK523: a novel *in vivo* tau imaging ligand for Alzheimer's disease

Michelle T. Fodero-Tavoletti,[1,2] Nobuyuki Okamura,[3] Shozo Furumoto,[3] Rachel S. Mulligan,[4] Andrea R. Connor,[1,2] Catriona A. McLean,[5] Diana Cao,[6] Angela Rigopoulos,[6] Glenn A. Cartwright,[6] Graeme O'Keefe,[4] Sylvia Gong,[4] Paul A. Adlard,[1,7] Kevin J. Barnham,[1,2,7] Christopher C. Rowe,[4] Colin L. Masters,[7] Yukitsuka Kudo,[8] Roberto Cappai,[1,2] Kazuhiko Yanai[3] and Victor L. Villemagne[4,7]

1 Department of Pathology, The University of Melbourne, Victoria, 3010, Australia
2 Bio21 Molecular and Biotechnology Institute, The University of Melbourne, Victoria, 3010, Australia
3 Department of Pharmacology, Graduate School of Medicine, Tohoku University, Sendai, 980-8575, Japan
4 Department of Nuclear Medicine and Centre for PET, University of Melbourne, Austin Health, Victoria, 3084, Australia
5 Department of Anatomical Pathology, The Alfred Hospital, Victoria, 3181, Australia
6 Ludwig Institute for Cancer Research, Austin Hospital, Victoria, 3084, Australia
7 The Mental Health Research Institute, Victoria, 3010, Australia
8 Innovation of New Biomedical Engineering Centre, Tohoku University, Sendai, 980-8575, Japan

Correspondence to: Victor L. Villemagne,
Austin Health, Department of Nuclear Medicine and Centre for PET,
145 Studley Road,
Heidelberg,
VIC, 3084, Australia
E-mail: villemagne@petnm.unimelb.edu.au

While considerable effort has focused on developing positron emission tomography β-amyloid imaging radiotracers for the early diagnosis of Alzheimer's disease, no radiotracer is available for the non-invasive quantification of tau. In this study, we detail the characterization of ^{18}F-THK523 as a novel tau imaging radiotracer. *In vitro* binding studies demonstrated that ^{18}F-THK523 binds with higher affinity to a greater number of binding sites on recombinant tau (K18Δ280K) compared with β-amyloid$_{1-42}$ fibrils. Autoradiographic and histofluorescence analysis of human hippocampal serial sections with Alzheimer's disease exhibited positive THK523 binding that co-localized with immunoreactive tau pathology, but failed to highlight β-amyloid plaques. Micro-positron emission tomography analysis demonstrated significantly higher retention of ^{18}F-THK523 (48%; $P < 0.007$) in tau transgenic mice brains compared with their wild-type littermates or APP/PS1 mice. The preclinical examination of THK523 has demonstrated its high affinity and selectivity for tau pathology both *in vitro* and *in vivo*, indicating that ^{18}F-THK523 fulfils ligand criteria for human imaging trials.

Keywords: tau; imaging; Alzheimer's disease; dementia; PET
Abbreviations: PiB = Pittsburgh Compound-B

Introduction

The clinical diagnosis of neurodegenerative diseases such as Alzheimer's disease is typically based on progressive cognitive impairments while excluding other diseases. However, clinical diagnosis is often challenging, with patients presenting with mild and non-specific symptoms attributable to diverse and overlapping pathologies that present as similar phenotypes (van der Zee *et al.*,

Received September 23, 2010. Revised December 21, 2010. Accepted January 10, 2011

2008). Consequently, definitive diagnosis of neurodegenerative diseases is still reliant on post-mortem examination.

Post-mortem examination of the Alzheimer's disease brain is characterized by gross cortical atrophy (Wenk, 2003). Microscopically, Alzheimer's disease is characterized by the presence of extracellular β-amyloid plaques and intracellular neurofibrillary tangles (Wisniewski *et al.*, 1989; Ho *et al.*, 1994). There has been much progress in developing PET imaging radiotracers for the non-invasive detection of β-amyloid deposition (Shoghi-Jadid *et al.*, 2002; Klunk *et al.*, 2005; Rowe *et al.*, 2007, 2008; Choi *et al.*, 2009). Recent reports indicate that the best characterized and successful imaging agent Pittsburgh Compound-B (PiB), preferentially binds to fibrillar β-amyloid contained within cored and compact plaques (Klunk *et al.*, 2004; Maeda *et al.*, 2007; Ikonomovic *et al.*, 2008) and with much lower affinity to the oligomeric forms of β-amyloid (Maezawa *et al.*, 2008) that are thought to be the toxic species of β-amyloid in Alzheimer's disease (Lambert *et al.*, 2001; Walsh *et al.*, 2002; Ferreira *et al.*, 2007; Cairns *et al.*, 2009).

While amyloid imaging PET studies confirmed that β-amyloid deposition occurs well before the onset of symptoms (supporting the hypothesis that this represents preclinical Alzheimer's disease), these studies also showed the lack of correlation between β-amyloid plaque deposition and cognitive impairment in Alzheimer's disease; suggesting that markers for different and downstream effects of β-amyloid may be better suited to assess disease progression (Jack *et al.*, 2010). Therefore, new ligands are needed to explore alternative biomarkers as specific indicators of neurodegeneration. Such agents may prove invaluable in the diagnosis, follow-up and therapeutic monitoring of Alzheimer's disease and other dementias.

An obvious biomarker is tau and in particular, abnormal deposits of hyperphosphorylated tau as neurofibrillary tangles, neuropil threads and as dystrophic neurites surrounding β-amyloid plaques (a pathological hallmark of Alzheimer's disease); however, tau deposits are also characteristic of a larger group of neurodegenerative diseases termed tauopathies [i.e. sporadic corticobasal degeneration, progressive supranuclear palsy, Picks disease, as well as frontotemporal dementia and parkinsonism linked to chromosome 17 (FTDP-17)] (Lee *et al.*, 2001). Unlike β-amyloid plaque deposition, human post-mortem studies indicate that neurofibrillary tangle density correlates with neurodegeneration and cognitive impairment (Duyckaerts *et al.*, 1987, 1990; Delaere *et al.*, 1989; Arriagada *et al.*, 1992; Dickson, 1997; McLean *et al.*, 1999). Futhermore, abundant neurofibrillary tangles are not observed in cognitively unimpaired individuals, in contrast to β-amyloid plaques that are present in some non-demented people (Katzman *et al.*, 1988; Delaere *et al.*, 1990; Rowe *et al.*, 2007, 2008). Moreover, CSF-tau and phospho-tau (ptau181) have been proven useful biomarkers in the diagnosis of Alzheimer's disease (Blennow and Hampel, 2003; Ganzer *et al.*, 2003; Hampel *et al.*, 2009*a*, *b*).

Despite the quantitative assessment of CSF levels of tau and phospho-tau being reliable biomarkers of neurodegeneration (Jack *et al.*, 2010), lumbar puncture is an invasive procedure for the widespread screening of the at-risk population. Additionally, CSF measures do not provide information on regional brain tau deposition that may have clear correlates with cognition (i.e. hippocampus) and therefore, might not be able to provide important information on the therapeutic outcomes or response to current drugs aimed at modulating tau/neurofibrillary tangles (Gozes *et al.*, 2009; Hampel *et al.*, 2009*a*, *b*; Wischik and Staff, 2009).

Molecular neuroimaging with tau-specific radiotracers may provide highly accurate, reliable and reproducible quantitative statements of global and regional brain tau burden, essential for the evaluation of disease progression, therapeutic trial recruitment and the evaluation of tau-specific therapeutics (for both Alzheimer's and non-Alzheimer's disease taupathies); where tau plays a central role. Certainly, the viability of imaging disease-specific traits has been demonstrated in recent years by PET ligands such as ^{11}C-PiB (Klunk *et al.*, 2004) and ^{18}F-FDDNP, used for imaging β-amyloid deposition. Unlike PiB, it has been suggested that FDDNP also binds to neurofibrillary tangles (Agdeppa *et al.*, 2001), which may contribute to ^{18}F-FDDNP retention in the mesial temporal cortex where β-amyloid-specific tracers such as ^{11}C-PiB scarcely bind (Kepe *et al.*, 2006; Ng *et al.*, 2007; Pike *et al.*, 2007; Rowe *et al.*, 2007).

Okamura and colleagues (2005) screened over 2000 small molecules to develop novel radiotracers with high affinity and selectivity for tau pathology/neurofibrillary tangles. Consequently, they identified a series of novel quinoline and benzimidazole derivatives that bind neurofibrillary tangles and, to a lesser extent, β-amyloid plaques. Serial analysis of those compounds led to the design and synthesis of a novel imaging agent, ^{18}F-THK523. The purpose of this study was to utilize a series of *in vitro*, *ex vivo* and *in vivo* techniques to determine whether ^{18}F-THK523 satisfied a number of radioligand criteria, assessing its suitability for the quantitative imaging of tau pathology in the human brain.

Materials and methods

Materials

All reagents were purchased from Sigma, unless otherwise stated. Human β-amyloid$_{1–42}$ was purchased from the W. M. Keck Laboratory (Yale University).

Mice

Mice were housed in conditions of controlled temperature (22 ± 2°C) and lighting (14:10 h light–dark cycle) with free access to food and water. rTg(TauP301L)4510 and their wild-type (CamKII) littermates were a kind gift from Jada Lewis (Dept Neuroscience, Mayo Clinic, Florida, USA) and APP/PS1 [B6C3-Tg(APPswe, PSEN1dE9)85Dbo/J] and wild-type littermates were purchased from JAX® Mice and Services. MicroPET studies employed 6-month-old rTg(TauP301L)4510 mice and 12-month-old APP/PS1 [B6C3-Tg(APPswe, PSEN1dE9)85Dbo/J] mice and their respective wild-type littermates.

Tissue collection and characterization

Human brain tissue was collected at autopsy. The sourcing and preparation of the human brain tissue was conducted by the Victorian Brain Bank Network. Alzheimer's disease pathological diagnosis was made according to standard NIA-Reagan Institute criteria (1997).

Determination of age-matched control cases were subject to the above criteria. Three Alzheimer's disease and three healthy, age-matched control cases were examined in this study.

^{18}F-labelling of THK523

Unlabelled THK523 and 2-(4-aminophenyl)-6-(2-tosyloxyethoxy)quinoline (BF241; the precursor for ^{18}F-THK523) were custom synthesized by Tanabe R&D Service Co. and confirmed for purity by reverse phase high-performance liquid chromatography, 1D nuclear magnetic resonance and mass spectrometry. ^{18}F-THK523 (Fig. 1) was synthesized by nucleophilic substitution of the tosylate precursor (BF-241). Following a 10-min reaction at 110°C, the crude reaction was partially purified on an activated Sep-Pak tC18 cartridge before undergoing semi-preparative reverse phase high-pressure liquid chromatography purification. Standard tC18 Sep-Pak reformulation produced ^{18}F-THK523 in >95% radiochemical purity. The radiochemical yield was 24% (non-decay corrected) and at end of synthesis, the average specific activity was 100 GBq/μmol (2.7Ci/μmol).

Measurement of octanol/water partition coefficient

^{18}F-THK523 (37 MBq) was added to a mixture of 3 ml 1-octanol and 3 ml of 1 M potassium phosphate buffer (pH 7.4). The mixture was shaken for 30 min, followed by centrifugation for 3 min. Aliquots (0.5 ml) were carefully taken from each phase for assay. The partition coefficient was calculated as follows: (count per minute/0.5 ml l-octanol)/(count per minute/0.5 ml buffer). Measurements were done in triplicate.

Generation and protein purification of K18Δ280 K-tau

K18Δ280 K-tau is a fragment of the full length protein, htau40 (Barghorn *et al.*, 2004; von Bergen *et al.*, 2006) comprising the four repeat regions of tau including residues 243–372. Polymerase chain reaction was implemented to generate K18Δ 280 K-tau from plasmids kindly provided by the Mayo Clinic. Δ280K refers to the deletion of the lysine residue at position 280. DNA encoding this region was cloned into expression vector pET15b at the NcoI and XhoI sites and transfected into BL21DE3 *Escherichia coli*. Ampicillin selected *E. coli* were lysed in buffer comprising 50 mM PIPES pH 6.9, 1 mM EDTA, 5 mM dithiothreitol and protease inhibitor cocktail (Roche), sonicated on ice (6 × 30 min, with 30 s rest intervals) and the lysate was then spun at 18 000*g* at 4°C for 15 min. The supernatant was removed and added to a solution of NaCl at a final concentration of 0.5 M. The sample was then boiled for 20 min prior to centrifugation using the abovementioned conditions. The supernatant was then applied to a PD10 column (Amersham) and equilibrated in equilibration buffer (50 mM Tris pH 8.2, 20 mM NaCl, 1 mM EDTA, 5 mM dithiothreitol) and filtered prior addition to a SP sepharose column. Protein fractions were then analysed by Coomassie staining and western blot and appropriate fractions containing a single tau band were pooled, buffer exchanged into water (PD10), lyophilized and stored at −80°C.

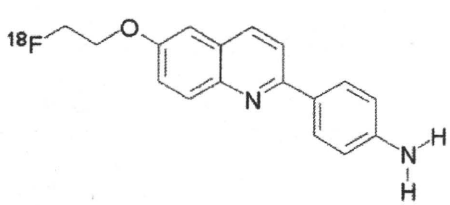

Figure 1 Chemical structure of ^{18}F-THK523 [2-(4-aminophenyl)-6-(2-fluoroethoxy)quinoline)].

Preparation of β-amyloid$_{1–42}$ and tau fibrils

Synthetic β-amyloid$_{1–42}$ was dissolved in 1 × phosphate buffered saline pH 7.7 to a final concentration of 200 μM. K18Δ280K-tau was dissolved in 1 × phosphate buffered saline pH 7.4 buffer to a final concentration of 20 μM. The solutions were then incubated at 37°C for 2 and 3 days, respectively, with agitation at 220 and 800 rpm, respectively (Orbital mixer incubator, Ratek). β-amyloid$_{1–42}$ fibril aggregation was confirmed via thioflavin T fluorescence spectroscopy and tau aggregation was confirmed by thioflavin S fluorescence spectroscopy; both fibril preparations were examined by transmission electron microscopy.

Thioflavin S/thioflavin T fluorescence

Aggregation of β-amyloid$_{1–42}$ fibril was confirmed using thioflavin T fluorescence (LeVine, 1999). Reactions (100 μl) comprising 20 μM β-amyloid$_{1–42}$ fibrils, 10 μM thioflavin T, 50 mM phosphate buffer were analysed at 444 nm (excitation) and 450–550 nm (emission), with an integration time of 1 s. K18Δ280K-tau fibril formation was confirmed by thioflavin S fluorescence whereby reactions comprising K18Δ280K-tau fibrils, 0.005% thioflavin S in 1 × phosphate buffered saline pH 7.4 were analysed at 440 nm (excitation) and 480 nm (emission), with an integration time of 1 s. Measurements were recorded using a Varian fluorescence spectrophotometer.

Transmission electron microscopy

Fibril formation of β-amyloid$_{1–42}$ and K18Δ280K-tau was further confirmed by transmission electron microscopy following staining with uranyl acetate. Carbon-coated copper electron microscopy grids were coated with K18Δ280K-tau or β-amyloid$_{1–42}$ fibrils, as described previously (Smith and Radford, 2001). Grids were viewed on a Siemens 102 transmission electron microscope, operating at a voltage of 60 kV.

In vitro ^{18}F-THK523 binding assays

Synthetic β-amyloid$_{1–42}$ or K18Δ280K-tau fibrils (200 nM) were incubated with increasing concentrations of ^{18}F-THK523 (1–500 nM). To account for non-specific binding of ^{18}F-THK523, the reactions described above were duplicated in the presence of unlabelled 1 μM THK523. The binding reactions were incubated for 1 h at room temperature in 200 μl of assay buffer [phosphate buffered saline, minus Mg^{2+} and Ca^{2+} (JRH Biosciences); 0.1% bovine serum albumin]. Separation of bound from free radioactivity was achieved by filtration under reduced pressure (MultiScreen HTS Vacuum Manifold; Multiscreen HTS 96-well filtration plates; 0.65 μm, Millipore). Filters were washed three times with 200 μl assay buffer and the radioactivity contained within the filters was counted in a γ-counter (Wallac 1480 Wizard 3"; Perkin Elmer). Binding data were analysed with curve fitting software that calculates the K_D and B_{max} using non-linear regression (GraphPad Prism Version 1.0, GraphPad Software). All experiments were conducted in triplicate.

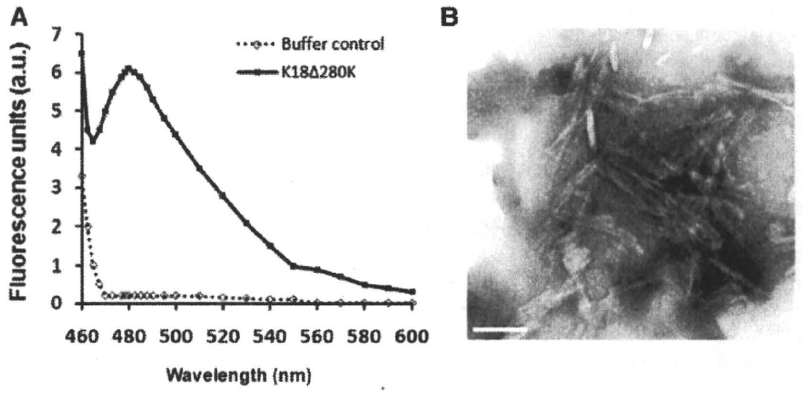

Figure 2 Characterization of K18Δ280K-tau fibrils. Recombinant K18(Δ280K)-tau was incubated with agitation (800 rpm) for 3 days at 37°C. (**A**) Graph depicting thioflavin S fluorescence, excitation/emission 440/480 nm, for K18Δ280K-tau (solid line) and no tau buffer control (dotted line). The graph for K18Δ280K-tau is indicative of positive amyloid fibril formation. (**B**) Electron microscopy image of K18Δ280K-tau fibrils. TechaniG^2 electron microscope; ×59 000 magnification. Scale bar: 50 nm. These data are representative of three independent experiments. a.u. = arbitrary units.

Immunohistochemistry and fluorescence analysis

Brain tissue from Alzheimer's disease and healthy control cases [three Alzheimer's disease (two female, one male), age range 75–83 years; three healthy controls (three female), age range 72–85 years], as well as mice (rTg4510, APP/PS1 and wild-type littermates) was fixed in 10% formalin/phosphate buffered saline and embedded in paraffin. For immunohistochemistry, 5 µm serial sections were deparaffinized and treated with 80% formic acid for 5 min and endogenous peroxidase activity was blocked with 3% hydrogen peroxide. Sections were then treated with blocking buffer (20% foetal calf serum, 50 mM Tris–HCl, 175 mM NaCl pH 7.4) before incubation with primary antibodies to β-amyloid (1E8; 1:50) or tau pAb (DAKO), for 1 h at room temperature. Serial 5 µm tissue sections were stained as follows: the first and third sections were immunostained with tau or 1E8 antibodies to identify tau tangles or β-amyloid plaques, respectively. The second serial section was stained with unlabelled THK523 to assess whether THK523 staining co-localized with the immunodetected tau tangles and/or β-amyloid plaques. Visualization of antibody reactivity was achieved with the LSAB™ kit (labelled streptavidin-biotin, DAKO) and sections were then incubated with hydrogen peroxidase-diaminobenzidine (H_2O_2-DAB) to visualize the tau tangles or β-amyloid-positive deposits. Sections were counterstained with Mayer's haematoxylin. To detect THK523 fluorescence, quenching was first performed whereby sections were first deparaffinized and tissue autofluorescence minimized by treatment of sections with 0.25% $KMnO_4$/phosphate buffered saline for 20 min prior to washing (phosphate buffered saline) and incubation with 1% potassium metabisulphite/1% oxalic acid/phosphate buffered saline for 5 min. Following autofluorescence quenching, sections were blocked in 2% bovine serum albumin/phosphate buffered saline pH 7.0 for 10 min and stained with 100 µM THK523 for 30 min. Washed (phosphate buffered saline) sections were then mounted in non-fluorescent mounting media (DAKO). Epifluorescence images were visualized on a Zeiss microscope [47CFP; filter set 47 (EM BP 436/20, BS FT 455, EM BP480/40)]. Co-localization of the THK523 and antibody signals was assessed by overlaying images from each of the stained serial tissue sections.

Autoradiography

For autoradiography, the hippocampal brain section of a patient with Alzheimer's disease (90-year-old female) was incubated with 2.2 MBq/ml of ^{18}F-THK523 at room temperature for 10 min and then washed briefly with water and 50% ethanol. After drying, the labelled section was exposed to a BAS-III imaging plate (Fuji Film) overnight. Autoradiographic images were obtained using a BAS-5000 phosphor imaging instrument (Fuji Film) with a spatial resolution of 25 × 25 µm. Neighbouring sections were immunostained using AT8 anti-tau monoclonal antibody (Innogenetics; diluted 1:20) or 6F/3D anti-Aβ antibody (DAKO; diluted 1:50).

Ex vivo biodistribution of ^{18}F-THK523

^{18}F-THK523 (0.68–1.32 MBq) was administered into the tail vein of ICR mice (n = 20, male, average weight 28–32 g). The mice were then sacrificed by decapitation at 2, 10, 30, 60 and 120 min post injection. The brain, blood and other organs were removed and weighed, and the radioactivity was counted with an automatic γ-counter. The percentage injected dose per gram (%ID/g) was calculated by comparison of tissue count to tissue weight. Each %ID/g value is an average ± SD of four separate experiments.

Small animal positron emission tomography imaging

All PET scans were conducted using a Philips MOSAIC small animal PET scanner with a transaxial spatial resolution of 2.7 mm full-width at half-maximum. Mice [n = 8 rTg4510 (four females, four males), n = 7 wild-type (four females, three males) mice and n = 3 APP/PS1 (all females) and three of their wild-type littermates (all females)] were intravenously injected with 100 µl of radiotracer comprising 3.7 MBq (0.35 µg/kg) of ^{18}F-THK523 via the tail vein. Mice were then anaesthetized using an isoflurane vaporizer with oxygen flow metre set to 5 l/min/5% isoflurane. Anaesthesia was maintained in a Veterinaire MINERVE anaesthetic assembly with the oxygen flow metre set to 2 l/min and vaporizer setting at 2%. A series of 6 × 5-min dynamic

emission scans were acquired starting at 5 min after injection. All images were reconstructed using a 3D row action maximum likelihood algorithm (RAMLA). Summed 25–35 min post-injection images were used for comparison between transgenic and wild-type mice. Image analysis was conducted using Wasabi v.2.0 software.

Statistical analysis

Normality of distribution was tested using the Shapiro–Wilk test and visual inspection of variable histograms. Statistical evaluations to assess differences in ^{18}F-THK523 binding were performed with analysis of variance (ANOVA) and a Tukey–Kramer Honestly Significant Difference test to establish differences between group means. Data are presented as mean ± SD unless otherwise stated.

Results

^{18}F-THK523 exhibits high affinity and selectivity for recombinant tau fibrils

To determine whether ^{18}F-THK523 satisfied the criteria of high affinity and selectivity for tau, the binding properties of ^{18}F-THK523 to tau fibrils was investigated and compared with β-amyloid$_{1-42}$ fibrils. A previously described truncated mutant of human tau, termed K18Δ280K-tau (Barghorn *et al.*, 2004; von Bergen *et al.*, 2006) that comprises the C-terminus of tau, including the four repeat regions and the FTDP-17 tau gene deletion resulting in the omission of lysine at position 280 (denoted Δ280K) was used for the studies. K18Δ280K-tau aggregates at low micromolar concentrations into paired helical filaments and straight filaments in the presence and absence of heparin (Perez *et al.*, 1996). Prior to conducting the binding assays, K18Δ280K-tau was formed into fibrillar structures (as monitored by thioflavin S fluorescence and transmission electron microscopy) by incubating 20 μM protein over 3 days at 37°C. On day 3, K18Δ280K-tau showed a thioflavin S fluorescence signal at ~480 nm (Fig. 2A), indicative of positive fibril formation. Fibril formation was confirmed by transmission electron microscopy with uranyl acetate staining (Fig. 2B). The β-amyloid$_{1-42}$ fibrils were generated as previously described (Fodero-Tavoletti *et al.*, 2007).

In vitro saturation studies were conducted using equimolar concentrations (200 nM, ~4.0×10^{-11} moles) of either K18Δ280-tau or β-amyloid$_{1-42}$ fibrils. While two classes of binding sites were identified on K18Δ280-tau fibrils (Fig. 3A) only one class of ^{18}F-THK523 binding sites was identified on β-amyloid$_{1-42}$ fibrils (Fig. 3B). Furthermore, there was a 10-fold higher affinity of ^{18}F-THK523 for the first class of K18Δ280-tau binding sites compared with β-amyloid$_{1-42}$ fibrils (Table 1). Overall, there was a ~5-fold higher number of ^{18}F-THK523 binding sites (B_{max}) on K18Δ280-tau fibrils, compared with β-amyloid$_{1-42}$ fibrils (Table 1).

THK523 demonstrates selectivity for tau pathology in sections of human hippocampal tissue

As a qualitative measure of its selectivity for tau pathology, THK523 recognition of tau pathology was assessed by histofluorescence and autoradiography. ^{19}F-THK523 and ^{18}F-THK523 share the same chemical structure, although ^{19}F is substituted for ^{18}F in the radiolabelled compound. For histofluorescence, unlabelled

Table 1 Binding parameters of ^{18}F-THK523 binding to fibrils

	K_{D1}	B_{max1}	K_{D2}	B_{max2}
K18Δ280K-tau fibrils	1.67	2.20	21.74	4.46
β-amyloid$_{1-42}$ fibrils	20.7	1.25		

K_D are in nM and B_{max} are in pmol ^{18}F-THK523/nmol fibrils.

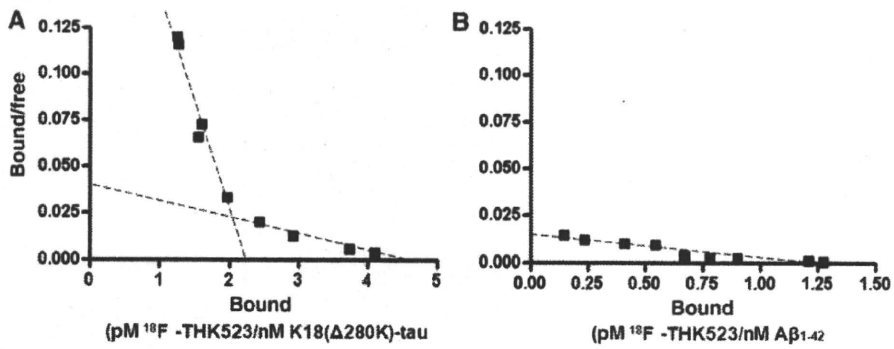

Figure 3 *In vitro* binding studies indicate two classes of ^{18}F-THK523-binding sites on K18Δ 280K-tau fibrils. Scatchard plots of ^{18}F-THK523 binding to synthetic K18Δ280K-tau (**A**) or (**B**) β-amyloid$_{1-42}$ fibrils. (**A**) Scatchard analysis identified two classes of THK523 binding sites on K18Δ280K-tau fibrils (K_{D1} and B_{max1} of 1.67 nM and 2.20 pmol THK523/nmol K18Δ280 K-tau, respectively; K_{D2} and B_{max2} of 21.7 nM and 4.46 pmol THK523/nmol K18Δ280 K-tau, respectively). (**B**) Scatchard analysis identified one class of THK523 binding sites on β-amyloid$_{1-42}$ with K_D and B_{max} of 20.7 nM and 1.25 pmol THK523/nmol β-amyloid$_{1-42}$. Binding data were analysed using GraphPad Software (Version 1.0). These data are the mean of three experiments for K18Δ280 K-tau and four experiments for β-amyloid fibrils.

THK523 binding to fixed serial sections from the hippocampus of subjects with Alzheimer's disease and age-matched controls was assessed. Contiguous sections were immunostained for β-amyloid and tau pathology with anti-β-amyloid and anti-tau antibodies, respectively. In all tissue sections examined, positive THK523 staining co-localized with tau pathology as detected in the contiguous tau immunostained section assessed (Fig. 4). THK523 failed to bind to diffuse β-amyloid plaques as indicated by the lack of co-localization with immunodetected β-amyloid pathology (Fig. 4). Likewise, autoradiography analysis in Alzheimer's disease hippocampal sections demonstrated that ^{18}F-THK523 bound to tau pathology with no ^{18}F-THK523 co-localization with immunodetected β-amyloid plaques (Fig. 5).

^{18}F-THK523 crosses the blood–brain barrier in mice

As well as being of low molecular weight (282.31 g/mol) and amenable to labelling with ^{18}F at high specific radioactivity [100 GBq/μmol (2.7 Ci/μmol)], a tau radiotracer should be adequately lipophilic to be able to cross the blood–brain barrier. The octanol/water coefficient ($logP_{oct}$) of ^{18}F-THK523 as a measure of lipophilicity, was calculated to be 2.91 ± 0.13. *Ex vivo* biodistribution studies of ^{18}F-THK523 in ICR mice, measured at 2, 10, 30, 60 and 120 min post injection, showed brain peak uptake of 2.75 ± 0.25% ID/g at 2 min post-intravenous injection (Fig. 6), indicating that ^{18}F-THK523 has adequate lipophilicity to cross the blood–brain barrier.

In vivo retention of ^{18}F-THK523 is significantly higher in tau transgenic mice brain compared with control and APP/PS1 mice

To further characterize ^{18}F-THK523 as a tau imaging radiotracer, *in vivo* microPET studies were performed to compare the retention of ^{18}F-THK523 in tau transgenic mice (rTg4510), versus their wild-type littermates (CamKII). Four independent studies were undertaken with 15 mice ($n = 8$ rTg4510 and $n = 7$ CamKII).

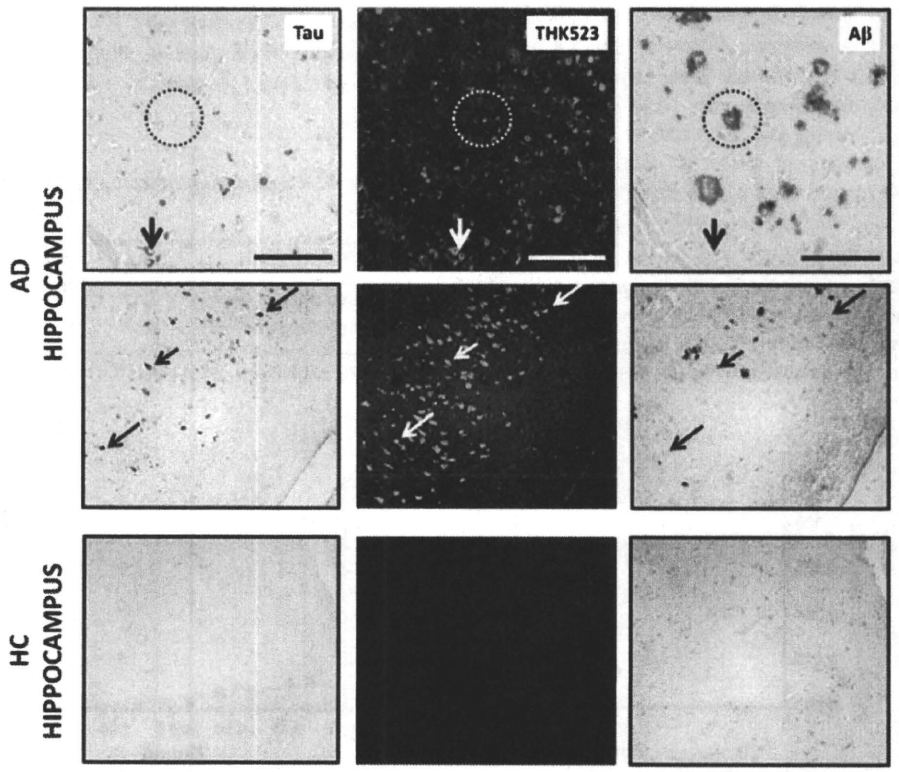

Figure 4 Histofluorescence analysis indicates that THK523 binds specifically to tau tangles with no detectable binding to β-amyloid plaques. Microscopy images of three serial sections (5 μm) from the hippocampus of a patient with Alzheimer's disease (AD) (*top* and *middle*) and a healthy control (HC) (*bottom*), immunostained with antibodies against tau (DAKO) and β-amyloid (1E8), to identify tau tangles and β-amyloid (Aβ) plaques, respectively; or stained with 100 μM THK523. Arrows indicate the location of tau tangles, while circles indicate the location of β-amyloid plaques. Positive THK523 staining appears to co-localize with tau immunostaining of neurofibrillary tangles in the hippocampus sections examined, but not to plaques. Tissue sections were imaged using a Zeiss microscope and Axiocam digital camera. Scale bars: 100 μm (*top*) and 200 μm (*middle* and *bottom*). These figures are representative of three subjects with Alzheimer's disease (two females, one male, age range 75–83 years) and three healthy controls (all female, age range 72–85 years).

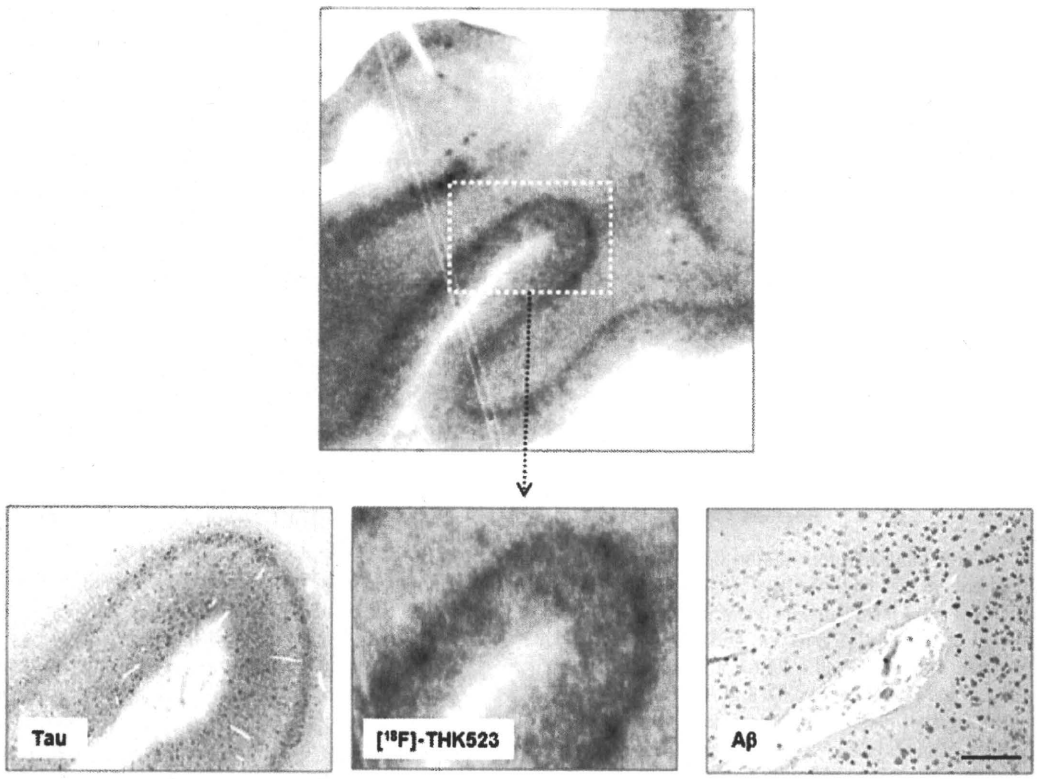

Figure 5 Autoradiography analysis indicates that ^{18}F-THK523 binds specifically to tau tangles with no detectable binding to β-amyloid plaques. (*Top*) ^{18}F-THK523 autoradiogram of Alzheimer's disease hippocampus (90-year-old female) serial section (low magnification). *Bottom*: microscopy images and autoradiogram (higher magnification) images of three serial sections (5 μm) from the hippocampus of the same Alzheimer's disease brain, immunostained with antibodies to tau (AT8, Innogenetics) and β-amyloid (6F/3D, DAKO), to identify tau tangles and β-amyloid (Aβ) plaques, respectively; or labelled with 2.2 MBq/ml ^{18}F-THK523. Positive ^{18}FTHK523 labelling appears to co-localize with tau immunostaining of neurofibrillary tangles in the hippocampus sections examined, but not to plaques. Scale bars: 500 μm. Autoradiographic images were obtained using a BAS-5000 phosphor imaging instrument (Fuji Film).

Representative microPET images are depicted in Fig. 7A and ^{18}F-THK523 time activity curves are depicted in Fig. 7C. Brain retention at ~30 min post injection of ^{18}F-THK523 was significantly higher (48%; $P < 0.007$) in the rTg4510 mice compared with their wild-type littermates (Fig. 7B). Analysis of bone, liver and intestine showed no significant differences in ^{18}F-THK523 retention (Fig. 7B), indicating a specific difference in brain uptake. Following microPET scanning, each mouse was euthanized and brains were harvested for biochemical and histofluorescence analysis. All rTg4510 mice brains examined were positive for tau overexpression as determined by western blot and immunohistochemical analysis (data not shown). Histofluorescence analysis of the same rTg4510 mice assessed by microPET identified positive THK523 staining that co-localized with immunopositive tau deposits (Fig. 8).

To further characterize the *in vivo* selectivity of ^{18}F-THK523 for tau pathology, microPET studies were conducted using the same experimental procedure in APP/PS1 transgenic mice ($n = 3$), exhibiting cerebral β-amyloid pathology but no tau deposits (Holcomb *et al.*, 1999). MicroPET analysis demonstrated that there was significantly lower retention of ^{18}F-THK523 in the brains of APP/PS1 mice, no different from the retention in their wild-type littermates ($n = 3$; Fig. 7B). Importantly, histofluorescence evaluation of rTg4510 and APP/PS1 brain tissue with 10 nM THK523 (a concentration that is achieved in the brain during PET studies), showed binding of THK523 to tau deposits in rTg4510 mice brains with negligible binding to β-amyloid plaques in the brain of APP/PS1 mice (Fig. 8).

Discussion

With the recent advances in instrumentation, image analysis and the development of new brain radiotracers, molecular neuroimaging with PET is rapidly expanding our knowledge base of neurodegenerative disease progression, improving early and accurate diagnosis, while promising to be effective in therapeutic monitoring and aiding in drug discovery and development. To date, much success has been achieved with β-amyloid radiotracers, in particular PiB being the best characterized radiotracer both *in vitro* and *in vivo*; showing selectivity for β-amyloid pathology resulting in a robust difference in ^{11}C-PiB brain retention in Alzheimer's disease

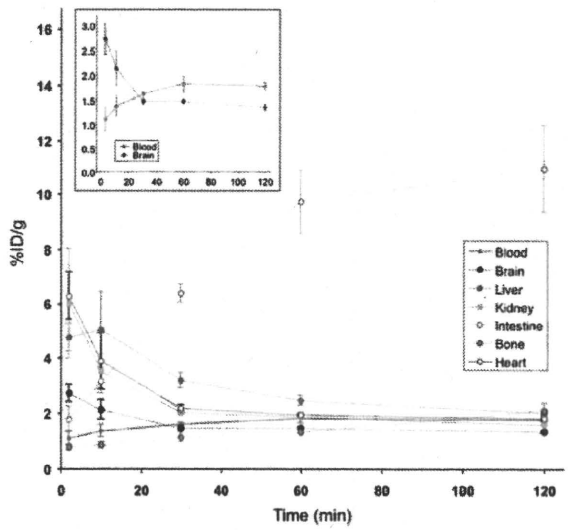

Figure 6 *Ex vivo* biodistribution studies of ^{18}F-THK523 in ICR mice. Initial uptake was highest (~6.2%ID/g) in the heart and kidney followed by a fast clearance. Liver radioactivity peaked (~5.0%ID/g) at 10 min after injection and was followed by a slow clearance, which mirrored a steady and substantial rise in radioactivity in the intestine (11%ID/g at 120 min after injection), suggesting that most of the tracer and/or its metabolites are eliminated through biliary excretion. There was a slow but steady increase in bone radioactivity, reaching a 2.1%ID/g at 120 min after injection, probably indicative of some degree of defluorination. The insert shows in better detail the brain and blood curves. Maximal ^{18}F-THK523 brain uptake (2.75%ID/g) was observed at 2 min after injection of the radiotracer, followed by a rapid clearance from the brain. Radioactivity in blood showed a different kinetic behaviour than the one observed in the brain, with a steady rise in radioactivity reaching an apparent plateau at about 60 min after injection. Uptake at each time point is expressed as percentage of injected dose per body weight (%ID/g) of ^{18}F-THK523. Curve represents the mean ± SD from four independent experiments. A total of 20 mice were examined.

compared with healthy aged-matched individuals in PET studies (Klunk *et al.*, 2004, 2005; Fodero-Tavoletti *et al.*, 2007, 2009). In addition to β-amyloid plaques, Alzheimer's disease brains are also pathologically characterized by the presence of tau pathology. Therefore, tau imaging may improve the specificity of diagnosis, allowing early detection of Alzheimer's disease and Pick's disease, where tau plays a role.

The identification and development of suitable PET radiotracer(s) is a demanding task especially given the considerable number of requirements that a radiotracer should fulfil to be deemed suitable for *in vivo* quantitative brain imaging. This study is the first to report a tau imaging radiotracer (^{18}F-THK523), that satisfies a number of criteria required for quantitative imaging of tau pathology in the human brain (Laruelle *et al.*, 2003; Nordberg, 2004; Pike, 2009). This study has shown that ^{18}F-THK523 has high affinity for recombinant tau fibrils and selectivity for tau fibrils/pathology over β-amyloid fibrils/pathology *in vitro*. Furthermore, it penetrates the blood–brain barrier, selectively highlighting tau pathology in the brains of rTg4510 tau transgenic mice *in vivo*.

In vitro saturation binding studies demonstrated that ^{18}F-THK523 binds to recombinant tau fibrils with high affinity in the low nanomole range. Typically ligands displaying affinities between 0.01–1.00 nM are deemed useful for *in vivo* quantitative PET studies. The high affinity ^{18}F-THK523-binding site (K_{D1}; 1.7 nM) exhibited >10-fold higher affinity compared with β-amyloid$_{1-42}$ fibrils (20.7 nM). Moreover, the number of high affinity ^{18}F-THK523-binding sites (K_{D1}) was almost 2-fold higher than the number of sites on β-amyloid$_{1-42}$ fibrils. In comparison to previous ^{3}H-PiB studies (Klunk *et al.*, 2005; Fodero-Tavoletti *et al.*, 2007), the affinity of ^{3}H-PiB for β-amyloid$_{1-42}$ (K_{D1}, 0.71–0.91 nM) is similar to the affinity of ^{18}F-THK523 for tau fibrils (K_{D1}, 1.7 nM). However, tau fibrils exhibit a larger number of ^{18}F-THK523 binding sites (B_{max1}, 2.20 pmol ^{18}F-THK523/nmol K18Δ280K-tau), compared with what has previously been reported for ^{3}H-PiB and β-amyloid$_{1-42}$ (1.01 pmol PiB/nmol β-amyloid$_{1-42}$) (Fodero-Tavoletti *et al.*, 2007). As the concentration of imaging radiotracers typically achieved during PET studies is in the low nanomole range, these findings strongly suggest that ^{18}F-THK523 will bind with high affinity and selectively to tau pathology under PET imaging conditions. Furthermore, as the brain area occupied by plaques is larger in comparison to neurofibrillary tangles, a >10-fold higher affinity and a larger number of ^{18}F-THK523-binding sites on tau/neurofibrillary tangles over β-amyloid plaques may prove essential in ascertaining a high tau signal over background in human PET studies (Laruelle *et al.*, 2003).

Further evidence of ^{18}F-THK523 selectivity for tau pathology was demonstrated by autoradiography and histofluorescence with positive THK523 staining, co-localizing with tau pathology and not with β-amyloid plaques in human Alzheimer's disease hippocampal sections. Importantly, even at THK523 concentrations 10 000-fold higher than those typically achieved under PET studies, THK523 failed to bind to diffuse plaques in the histofluorescence studies. There was some inconsistent staining of cored/compact plaques, suggesting that there might be some ^{18}F-THK523 binding to cored β-amyloid plaques, but only under non-PET radiotracer conditions. Similarly, variable staining of neurofibrillary tangles at high concentrations of PiB, has been reported by Ikonomovic and colleagues (2008).

In addition to high affinity and selectivity, a suitable tau radiotracer must be able to cross the blood–brain barrier to reach its target *in vivo*. The small size (molecular weight <450) (Laruelle *et al.*, 2003) and lipophilic nature of ^{18}F-THK523 [log P_{OCT} value of 2.9 ± 0.1; $-\log P_{OCT}$ values in the range of 0.9 and 3.0, show optimal entry into the brain (Dishino *et al.*, 1983)] indicates that ^{18}F-THK523 is able to penetrate the blood–brain barrier. This was confirmed in both *ex vivo* biodistribution and *in vivo* microPET imaging studies. Additionally, microPET imaging demonstrated that ^{18}F-THK523 retention was significantly higher (48%; $P = 0.007$) in the brains of rTg4510 tau transgenic mice compared with their control littermates, devoid of tau pathology; in agreement with the *in vitro* saturation and histofluorescence studies. Moreover, selectivity of THK523 for tau pathology was further supported by the ^{18}F-THK523 microPET assessment of APP/PS1 mice. These mice possess substantial cerebral β-amyloid plaque

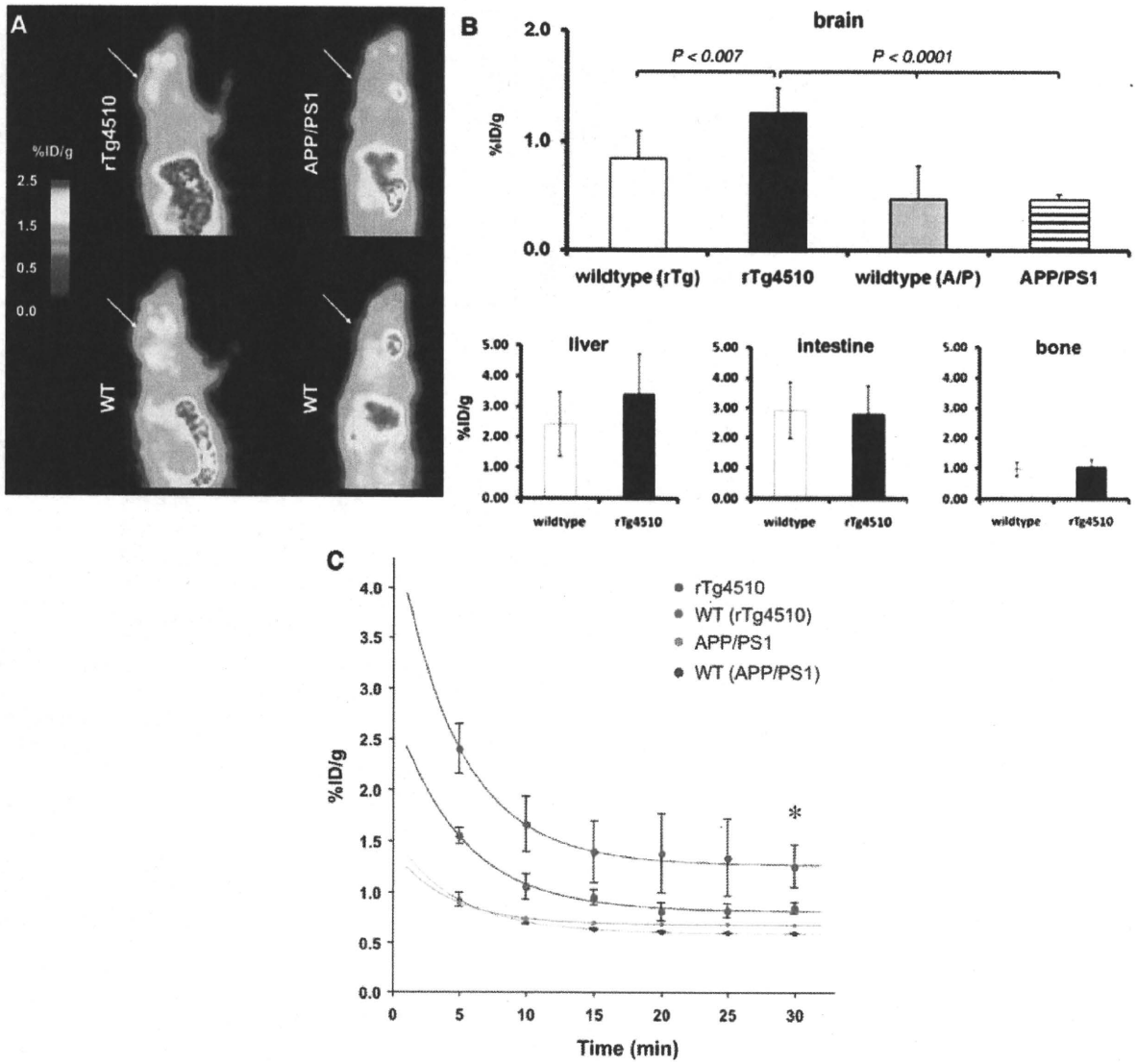

Figure 7 *In vivo* ^{18}F-THK523 microPET studies of tau and β-amyloid overexpressing transgenic mice. (**A**) Representative microPET scans at 30-min post injection of ^{18}F-THK523. rTg4510 mice (*top, left*) exhibited higher ^{18}F-THK523 brain retention compared with their wild-type (WT) littermate (*bottom, left*). Low ^{18}F-THK523 retention was observed APP/PS1 (*top, right*) versus their wild-type littermates (bottom, right). (**B**) Analysis of the ^{18}F-THK523 brain microPET data (30-min post injection) in rTg4510, APP/PS1 mice and their respective wild-type littermates revealed significantly higher (*) retention of ^{18}F-THK523 in the brain (*top*) of rTg4510 mice compared with APP/PS1 mice as well as their respective wild-type littermates. No significant differences in ^{18}F-THK523 retention were observed in the liver, intestine and bone (*bottom*). Data are presented as mean ± SD. (**C**) Brain time-activity curves of ^{18}F-THK523 microPET data expressed as percentage of injected dose per body weight (%ID/g) of ^{18}F-THK523 at each time point. Curve represents the mean ± SD of four independent studies employing $n = 8$ rTg4510 (four females, four males), $n = 7$ WT (four females, three males) mice and $n = 3$ APP/PS1 (all females) and three of the wild-type (all females) mice. Data are presented as mean ± SD.

load; however, the retention of ^{18}F-THK523 in these mice was significantly lower than in rTg4510 tau transgenic mice and not different from the retention in CamKII mice or their own wild-type littermates; suggesting that THK523 does not significantly bind to β-amyloid plaques and is selective for tau pathology *in vivo*.

Analysis of ^{18}F-THK523 biodistribution in the microPET studies showed no significant differences in ^{18}F-THK523 retention in the liver, intestine or bone between rTg4510 tau transgenic and wild-type mice. ^{18}F-THK523 retention in bone is indicative of some degree of defluorination (Van Dort *et al.*, 1995). *In vitro* stability testing showed that ^{18}F-THK523 was stable *in vitro*, suggesting that defluorination most likely occurs post-injection (data not shown). However, as the degree of free ^{18}F-bone retention is similar in both transgenic and control mice, the free ^{18}F does not